



Strathprints Institutional Repository

Mizzi, Kurt and Demirel, Yigit Kemal and Banks, Charlotte and Turan, Osman and Kaklis, Panagiotis and Atlar, Mehmet (2017) Design optimisation of Propeller Boss Cap Fins for enhanced propeller performance. *Applied Ocean Research*, 62. 210–222. ISSN 0141-1187 , <http://dx.doi.org/10.1016/j.apor.2016.12.006>

This version is available at <http://strathprints.strath.ac.uk/59053/>

Strathprints is designed to allow users to access the research output of the University of Strathclyde. Unless otherwise explicitly stated on the manuscript, Copyright © and Moral Rights for the papers on this site are retained by the individual authors and/or other copyright owners. Please check the manuscript for details of any other licences that may have been applied. You may not engage in further distribution of the material for any profitmaking activities or any commercial gain. You may freely distribute both the url (<http://strathprints.strath.ac.uk/>) and the content of this paper for research or private study, educational, or not-for-profit purposes without prior permission or charge.

Any correspondence concerning this service should be sent to Strathprints administrator: strathprints@strath.ac.uk



Design optimisation of Propeller Boss Cap Fins for enhanced propeller performance

Kurt Mizzi*, Yigit Kemal Demirel, Charlotte Banks, Osman Turan,
Panagiotis Kaklis, Mehmet Atlar

Department of Naval Architecture, Ocean and Marine Engineering, University of Strathclyde, 100 Montrose Street, Glasgow, G4 0LZ, UK



ARTICLE INFO

Article history:

Received 16 March 2016

Received in revised form

28 November 2016

Accepted 9 December 2016

Keywords:

Propulsion efficiency

Computational fluid dynamics

PBCF

Optimisation

ABSTRACT

Economic pressures and regulatory requirements have brought about a great interest in improving ship propulsion efficiency. This can be exercised by installing Energy Saving Devices (ESD) such as Propeller Boss Cap Fins (PBCF). This paper demonstrates an approach for optimising PBCF by using Computational Fluid Dynamics (CFD) analysis. The conducted Reynolds-averaged Navier-Stokes (RANS) CFD open water model tests were validated by comparison with experimental data until the simulation was deemed satisfactory within the capabilities and limitations of the model. A design and optimisation procedure was defined to analyse the impact of ESDs on propeller efficiency and then used to evaluate the influence of alternative geometric parameters and locations of the PBCF on the hub. This analysis was done at full scale using high fidelity CFD-based RANS methods. Outcomes of the study include a design and optimisation process that can be used for the analysis of other ESDs on the market. The influences of various PBCF geometry were examined with optimal solutions presented for the analysis case. Results indicated a net energy efficiency improvement of 1.3% contributing to a substantial minimisation of cost and energy consumption. A reduction in the hub vortex was also clearly identified and presented.

© 2016 The Author(s). Published by Elsevier Ltd. This is an open access article under the CC BY license (<http://creativecommons.org/licenses/by/4.0/>).

1. Introduction

The first international ship energy efficiency regulations entered into force in 2013 with a phased implementation plan [1]. This has brought about the need for improving energy efficiency for environmental benefits that will also help reduce operational costs during difficult maritime economic cycles [2]. Although shipping is known to be the most efficient mode of commercial transportation per tonne of cargo, several design and operational methods have been identified with the potential to increase ship energy efficiency [3]. Whilst the ambition to increase energy efficiency is shared with shipping companies seeking to reduce fuel costs and operational expenses, one of several barriers [4] towards adopting and implementing different Energy Saving Devices (ESDs) is the lack of known reliable performance and hence low confidence about their reliability.

Ship energy consumption depends on the performance of different components of the ship system; one significant element being the ships' hydrodynamic system comprising hull resistance,

propulsion efficiency and hull-propeller interaction. Several studies [5–8] suggest that the installation of an ESD on a ship can result in a significant improvement in energy efficiency. Ongoing research focuses on maximising the energy efficiency potential of these devices through design improvements and, with the increased availability of computational power and advances in numerical tools and modelling software, the use of optimisation procedures are becoming increasingly popular for doing this.

Propeller Boss Cap Fins (PBCF) are an energy saving device that can enhance propeller efficiency, thus requiring less power to propel the vessel forward at a certain speed. The primary function of PBCF is to improve the propeller performance characteristics, via, but not limited to, minimising the hub vortex and resultant rudder cavitation.

Most of the previous PBCF research has been conducted experimentally at model scale conditions analysing different PBCF parameters independently and seeking the local optimum by analysing different case studies. Investigating ESDs using model-scale experimental methods give rise to some extrapolation issues. For example, energy saving devices are generally fitted within the boundary layer of the hull and are strongly affected by viscous effects that cannot be directly extrapolated to full scale conditions. Some studies have indicated that ESDs tend to be more efficient

* Corresponding author.

E-mail address: kurt.mizzi@strath.ac.uk (K. Mizzi).

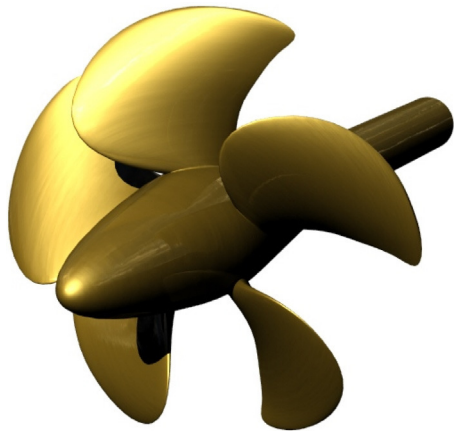


Fig. 1. PPTC Propeller.

at full scale than model scale [5,6]. ESD investigation, optimisation and analyses should therefore be performed at full scale to minimise uncertainties and error [9]. Furthermore, using experimental methods requires extensive resources and time, only allowing for a limited number of designs to be analysed. However, it is also difficult to analyse a vast range of design candidates at full scale using accurate numerical methods due to computational limitations. A common approach is to therefore run various designs with a less demanding numerical model, followed by further optimisation on promising design candidates employing more accurate simulations, such as CFD. However, a concern with the optimisation of promising design candidates is the consideration of the PBCF parameters independently that might result in local optima solutions being found and not necessarily the global optimum. To the best of authors' knowledge, no study has yet focused on optimising PBCF fins at full scale using RANS CFD methods seeking the global optimum for maximum savings by taking into consideration a number of parameters that might be dependent on each other.

The key objective of the study is to propose a novel full scale PBCF design optimisation approach using a coupled optimiser-CFD framework with the aim to improve propulsion efficiency and thus help the energy efficiency of a vessel. The various geometric design candidates were run in submerged water conditions of uniform flow using Reynolds-Averaged Navier-Stokes (RANS) equations to simulate open water tests, and analysed to predict the ESD impact on the propulsive efficiency. The numerical model was then coupled to an optimisation parametric modeller (CAESES®) that was used to analyse 120 different PBCF designs at full-scale. In addition, this study sought to find the global optimal PBCF design considering a number of interdependent parameters.

The paper is organised as follows: Section 2 gives a brief literature review describing various experimental and numerical open-water test methods as well as looking into various PBCF studies and deductions. All geometry details are then presented in Section 3 while in Section 4, the numerical modelling and computational methods are described. The optimisation algorithms and methods used, together with the procedure of the parametric study, are then outlined in the Section 5. The verification study and optimisation results are then demonstrated in Section 6 while discussed with any concluding remarks in the final section are provided.

2. Background

2.1. Propulsion efficiency

A propeller's performance characteristics can be expressed in term of its open water and after-hull properties. The former indi-

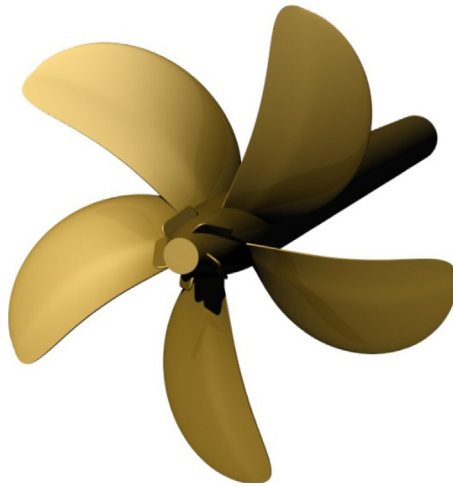


Fig. 2. CAESES Propeller with PBCF.

Table 1
PPTC Propeller Parameters [22] (SVA Potsdam Model Basin, 2011).

VP1304		
Type	Pitch Propeller	
Diameter (m)	D	0.250
Pitch Ratio	$P_{0.7}/D$	1.635
Area Ratio	A_E/A_0	0.779
Chord Length (m)	$C_{0.7}$	0.104
Skew (deg)	θ	18.837
Hub Ratio	D_h/D	0.300
No. of Blades	Z	5
Rotation	Direction	Right
Revolutions/sec (rps)	n	15

cates the behaviour of the propeller in uniform flow with a steady load, whilst the latter, as the name suggests, describes moment and forces for a propeller in a mixed wake field experiencing steady and unsteady loads. Propeller designs are generally compared by analysing their thrust (T) and torque (Q) in an open water environment. These parameters are subsequently non-dimensionalised; as one can readily see from (1)–(4), the so-called thrust (K_T) and torque (K_Q) coefficients can be used to evaluate the propulsion efficiency (η_0),

$$K_T = \frac{T}{\rho n^2 D^4} \quad (1)$$

$$K_Q = \frac{Q}{\rho n^2 D^5} \quad (2)$$

$$J = \frac{V_A}{nD} \quad (3)$$

$$\eta_0 = \frac{JK_T}{2\pi K_Q} \quad (4)$$

where D is the propeller diameter, ρ is the water density, V_A the advance velocity and n denotes the revolutions per second.

Thrust and torque coefficients can be plotted for a range of advance coefficients (J) producing propeller curves, from which the optimum efficiency and operating point of a propeller can be identified. It should be noted that the open water propeller curves are only applicable for uniform flow simulations, implying that the propeller is submerged and rotated in an isolated water environment with a constant uniform flow of velocity (V_A). Once fitted behind a vessel, oncoming flow from the stern is non-uniform, thus changing propeller performance. Nevertheless, open water charac-



Fig. 3. PBCF Geometry.

teristics can be considered to offer a useful initial indication of a propeller's behaviour.

2.2. Open water test methods

Propeller performance is traditionally predicted by carrying out experimental open water tests at model scale which tends to be time-consuming. Recently, numerical methods have been widely introduced. They are generally cheaper and more efficient, making them ideal for use at the initial design stages of a ship, before moving onto the more reliable and expensive experimental tests later in the design. With these methods, various designs can be numerically analysed before identifying the optimal solution to be run experimentally, saving cost and time. Among the various numerical methods developed so far, the most common are the Boundary Element Methods (BEM) and Reynolds-Averaged Navier-Stokes (RANS) computations. Bertram [10] indicates that although BEM's physical model is considerably simpler than that of RANS, computing the strength of the singularities (dipoles and/or sources) distributed over the propeller blade is relatively complex and the flow prediction at the tip is not accurately captured due to the inviscid approach. Hsin et al. [11] add that the BEM is incapable of accurately capturing the viscous effects such as the boundary layer and flow separation, thus failing to properly predict the propeller performance. On the other hand, with regard to RANS methods, Bertram [10] outlines the benefits of simulating viscous effects for predicting flow details but at the expense of cost and computational time. With the advance of technology, computational power and the development of commercial Computational Fluid Dynamics (CFD) code, RANS simulations are considered to be the preferred practice in modern times. However, as described by Queuteu [12], the combinations of BEM-RANS methods for preliminary design stages have also been considered due to their computational cost benefits.

Appropriate selection of mesh size and structure and the right physics models are all important to develop adequate CFD RANS simulations that produce accurate results. Nakisa et al. [13] investigated the different models and indicate that the Shear Stress Transport (SST) $k-\omega$ turbulence model, together with a sliding mesh domain produced the better results. These results were compared

Table 2
Ceases Parameters.

Profile	Naca66
Rev Per Sec (rps)	n
Rev Per Minute (rpm)	n
Diameter (m)	D
Hub Ratio	D_h/D
Number of Blades	Z
Direction	Rotation
Pitch Ratio	$P_{0.7}/D$
Rake(m)	$R_{0.7}$

Table 3
MRF vs Sliding Mesh.

$J=1$	K_T	$10 K_Q$
MRF	0.38604	0.96894
SM	0.38595	0.96885

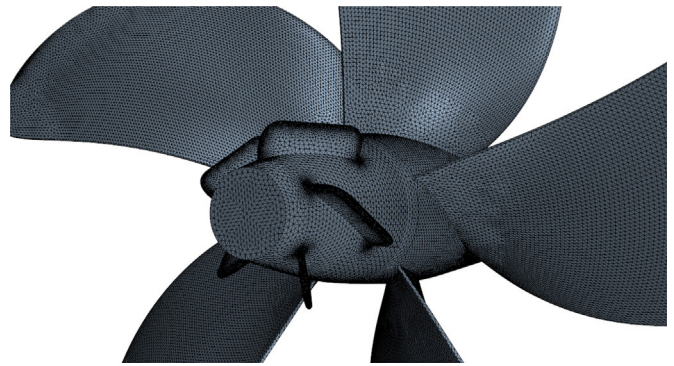
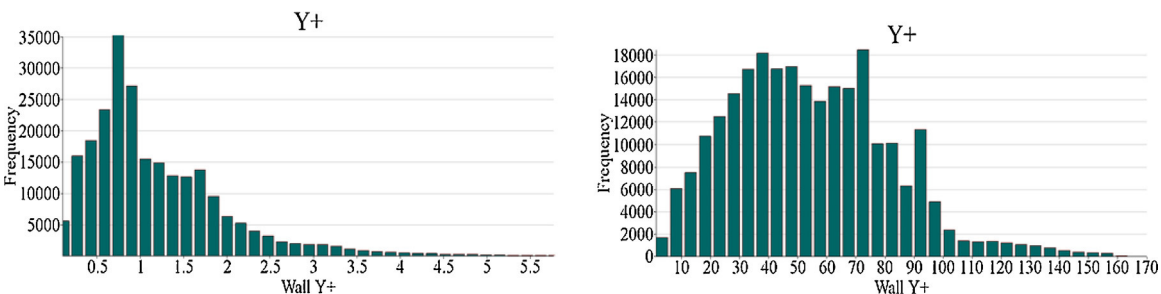


Fig. 4. Surface Mesh for CAESES Propeller with PBCF.

to experimental values producing an average error of 8% for K_T , 13% for K_Q and 11% for η_0 . The authors [13] also outlined that the errors increase in extreme load conditions. This is in good agreement with Da-Qing's [14] remarks indicating that the error difference between his experimental and numerical results for K_T and K_Q are 3% and 5% respectively within a certain range of the advance coefficient J , with the error increasing outside these conditions. He also adds that grid refinement has no significant effect on the propeller performance characteristics; however, it produces different results for local flow quantities. Da-Qing [14] states that in general, K_Q is over predicted and that the difference in error prediction is larger than that of K_T . He supports the reasoning by indicating the lack of transition model in the RANS solver. It is known that, the boundary layer over the blade in model scale conditions is rarely fully turbulent due to the low Reynolds number resulting in laminar flow. The fully turbulent models generate strong turbulent viscosity and shear stresses on the blade surfaces hence over predicting the skin coefficient resulting in an over predicted K_Q and under predicted K_T . However, Arikhan [15] analysed a podded propeller in a similar manner that produced a greater error for thrust than torque. This could be due to the highly skewed propeller resulting in very little laminar flow.

Krasilnikov [16] indicates that the International Towing Tank Conference (ITTC) scaling methods are not accurate in predicting the Reynolds number effect at full scale. He studied the scale effects on propellers with different magnitude of skew in turbulent flow. Results indicated that laminar regions on the blade are smaller for higher skew blades. It was concluded that the scale effects in open water models were found to be dependent on the blade geometry and the propeller load which could be explained by the variation

Fig. 5. Y^+ Histogram (Model and Full Scale Respectively).**Table 4**
Steady vs Unsteady.

$J = 1$	K_T	$10 K_Q$
Steady MRF	0.38623	0.96916
Unsteady MRF	0.38604	0.96895

in magnitude of pressure and friction components. He also stated that the inaccuracy of CFD procedures is also due to the negligence of roughness effects which in general can be introduced as correction factors for full scale models. Nevertheless, it has recently been shown in [17–19] that the effect of surface roughness can be accurately simulated using modified wall functions in CFD software and that the effect of coatings and fouling can be investigated.

2.3. Propeller Boss Cap Fins

There are different ways to improve the propulsion efficiency of a vessel. The choice of methodology highly depends on the case study in question. The propulsion efficiency of new vessels can be improved by hull and propeller design optimisation procedures at the design stage, while existing vessels require different retrofit solutions; such as the installation of an ESD to the hull stern or to the propeller system. One particular, well-established ESD is the Propeller Boss Cap Fin, more commonly known as a PBCF. As the name implies, a PBCF is a post – swirl fin that is installed onto the boss cap of the propeller. It is well known that a propeller produces a hub vortex which reduces the propeller efficiency and may cause rudder corrosion. As Ghassemi [20] explains, the strength of such phenomena is dependent on the hub geometry as well as the axial load distribution of the propeller. The aim of installing a PBCF is to minimise this hub vortex, increase propeller efficiency and reduce fuel costs. Having installed more than 3000 of this technology on vessels, MOL Techno-Trade Ltd. [21] claims up to 5% fuel savings.

Nojiri et al. [5], Hansen et al. [6] and Atlar et al. [7] all come to the common agreement about the beneficial effects of using PBCF resulting in a reduction in shaft power and subsequent increase in fuel efficiency. Hsin et al. [11] point out that the number of fins should be the same as the propeller blade number and that their radius should be 20–25% of the propeller radius. In addition to this, Hsin et al. also reveal that the optimum axial position is 5% of the propeller radius. Ghassemi et al. [20] add that the fins should be

placed in such a way that the leading edge is positioned between the roots of two adjacent blades.

3. Geometry

3.1. Validation study

Validation studies (see Section 4) were carried out using an open source, model-scale, controllable pitch propeller in a pull test configuration, designed by SVA [22] shown in Fig. 1. SVA provide the experimental open water test results allowing comparison and validation of our simulation model. The design parameters for this Potsdam Propeller Test Case (PPTC) propeller can be seen in Table 1 below.

3.2. Propeller with PBCF study

Once validated (see Section 6), analysis was conducted using a custom constant pitch full-scale propeller and parametric PBCF, designed with the aid of the NURBS modeller tool CAESES provided by Friendship Systems. For the purposes of this study, the propeller illustrated in Fig. 2 will be referred to herein as the CAESES propeller. Parameters and dimensions were adjusted according to the requirements of this study. The CAESES Propeller details can be found in Table 2.

The PBCF as shown in Fig. 3 were designed in such a way that resulted in a parametric model incorporating appropriate design variables, namely fin length, angular fin position, fin thickness, fin pitch angle and fin height. These parameters were considered the most important based on the literature.

4. Numerical modelling

The open water CFD model used for the PBCF study was first validated using the model-scale Potsdam VP1304 propeller in numerical software. In this study a Reynolds-Averaged Navier-Stokes (RANS) approach was applied using the commercial CFD software Star-CCM+® version 9.0.2, which was developed by CD-Adapco [23]. The super computer at the University of Strathclyde was utilised to allow faster and more complex simulations. During the validation study, various physics models and meshes were tested identifying the optimality criteria for the simulation that resulted in the most accurate propeller characteristics (see Section

Table 5

Mesh Size Comparison for PPTC Model-Scale Propeller.

	Coarse			Medium			Fine		
$Cell\ Number$	4.59 M			6.5 M			9.2 M		
$J = 1$	KT	KQ	η_0	KT	KQ	η_0	KT	KQ	η_0
Results	0.3798	0.0960	0.6297	0.3843	0.0967	0.6324	0.3862	0.0969	0.6343
Accuracy (%)	95.09	98.47	96.57	96.22	99.20	97.00	96.70	99.41	97.28

*Accuracy (%) represents the difference between the numerical results and the experimental values.

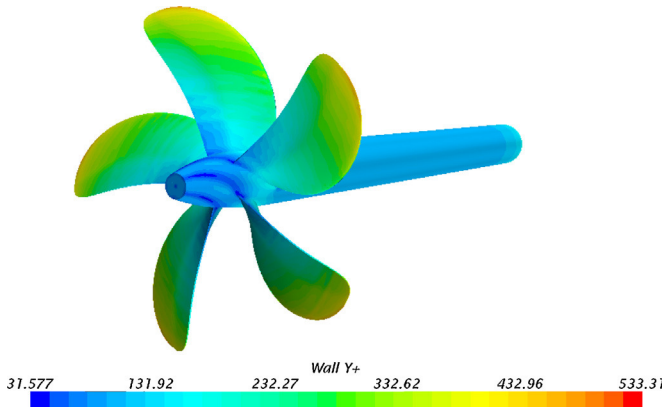


Fig. 6. Y^+ values (full-scale CAESES).

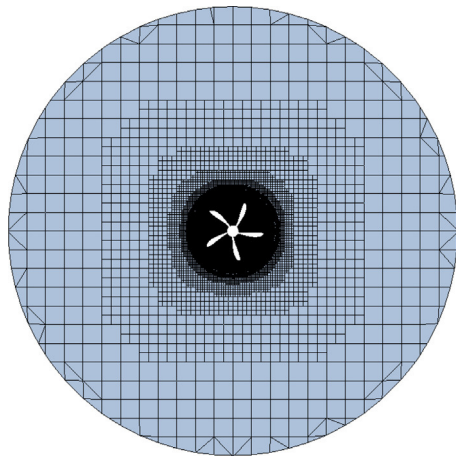


Fig. 7. Mesh Refinement.

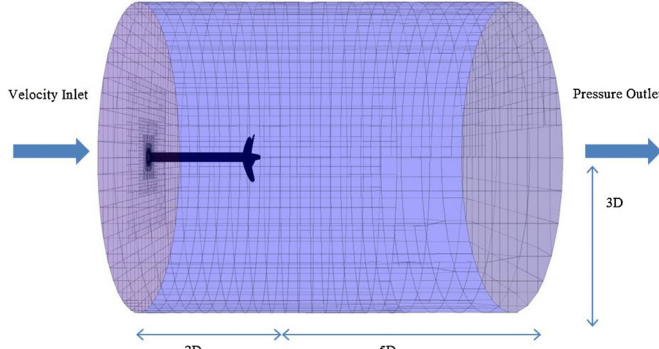


Fig. 8. Boundary Conditions.

4.2 and 4.3). Once validated, the same physics, mesh and setup were used to analyse the CAESES propeller in full-scale conditions.

4.1. Physics

A Reynolds-Averaged Navier-Stokes (RANS) solver was used to solve governing equations and to simulate a three-dimensional environment using the SST (Shear Stress Transport) $k-\omega$ model assuming a turbulent flow. This turbulence model is a two-equation eddy-viscosity model that enriches the $k-\omega$ model with an additional non-conservative cross-diffusion term that potentially makes the model produce similar results to that of the $k-\varepsilon$ model, thus enabling the system to have the best of both worlds.

Table 6
Wall Y^+ Study.

	$Y^+ < 1$			$Y^+ > 30$		
$J = 1$	KT	KQ	η_0	KT	KQ	η_0
Error (%)	3.30	0.59	2.72	4.19	-0.62	4.78

*Error (%) represents the difference between the numerical results and the experimental values.

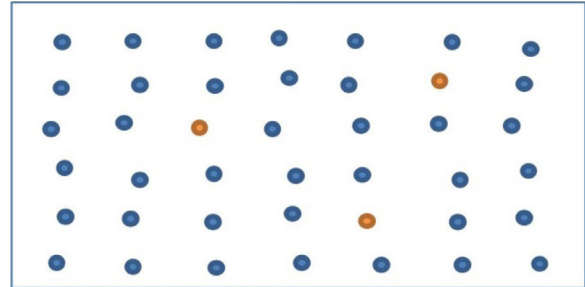


Fig. 9. Quasi-Random Sequence.

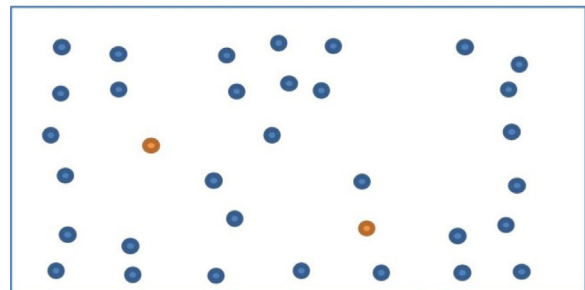


Fig. 10. Random Sequence.

This blends the ε approach in the far field and the ω model in the inner field near the solid boundaries, making it suitable for adverse pressure gradients and separating flows [23]. Steady state simulations were run for a sufficient number of iterations to ensure proper convergence. For those cases of unsteady sliding mesh simulations during the validation studies, the time step was set to rps/200 as recommended by the ITTC [24].

The governing equations were discretised using a Finite Volume Method with the velocity-pressure coupling being handled using a SIMPLE algorithm. A second order convection scheme was used for the momentum equations and a first order temporal discretisation was used. The flow equations were solved in a segregated manner. The continuity and momentum equations were linked with a predictor-corrector approach. The propeller was placed in an immersed incompressible water liquid environment of constant density and segregated flow represented by the following continuity and momentum flow equations [25] given in tensor notation and Cartesian coordinates by (5) and (6),

$$\frac{\partial(\rho\bar{u}_i)}{\partial x_i} = 0 \quad (5)$$

$$\frac{\partial(\rho\bar{u}_i)}{\partial t} + \frac{\partial}{\partial x_j}(\rho\bar{u}_i\bar{u}_j + \rho u_i \bar{u}_j) = -\frac{\partial \bar{p}}{\partial x_i} + \frac{\partial \bar{\tau}_{ij}}{\partial x_j} \quad (6)$$

where ρ is density, \bar{u}_i is the averaged Cartesian components of the velocity vector, $\rho u_i \bar{u}_j$ is the Reynolds-stress tensor and \bar{p} is the mean pressure. Finally, $\bar{\tau}_{ij}$ denotes the mean viscous-stress tensor defined below as

$$\bar{\tau}_{ij} = \mu \left(\frac{\partial \bar{u}_i}{\partial x_j} + \frac{\partial \bar{u}_j}{\partial x_i} \right) \quad (7)$$

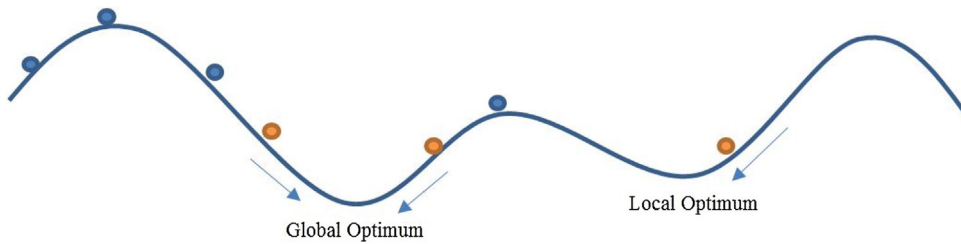


Fig. 11. Optimisation Algorithm.

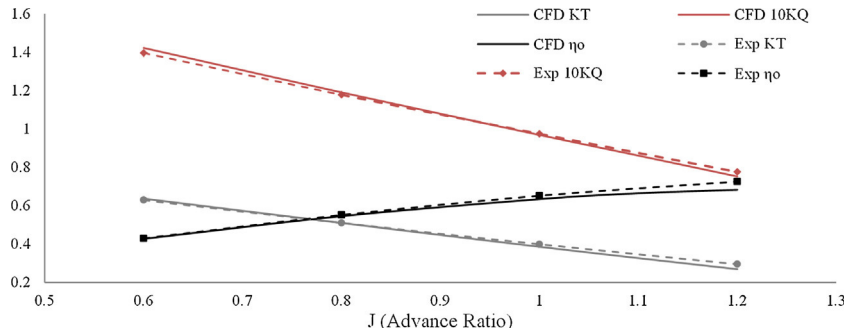


Fig. 12. PPTC Open Water Characteristics.

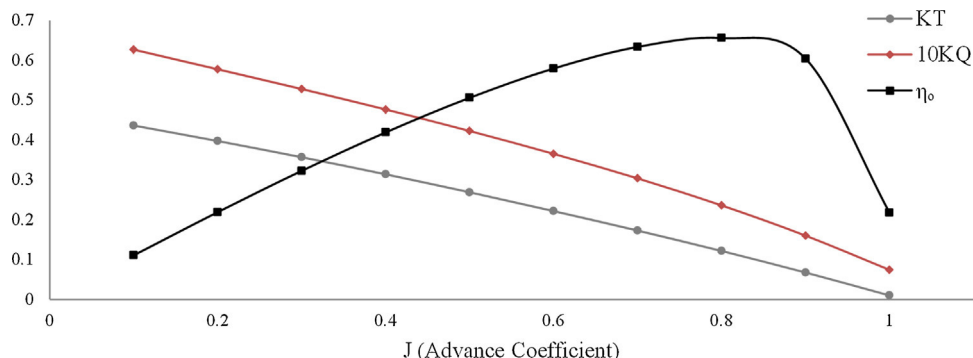


Fig. 13. CAESES Open Water Characteristics.

with μ being the dynamic viscosity.

4.2. Modelling variations

In CFD work, a rotating propeller can be simulated using different models, namely the Moving Reference Frame (MRF) method and the Rotating Mesh also known as the Sliding Mesh approach. As the name suggests, for the Rotating Mesh, the domain rotates about an axis yielding transient calculations producing time-accurate results that require high computational power. Meanwhile, with regards to the less computationally intensive MRF approach, the domain remains stationary with an assigned frame of reference rotating about a pre-defined axis with respect to the global coordinate system. This type of simulation carries out a steady-state approximation to a transient problem producing time-averaged results. When running unsteady simulations, the MRF approach generally provides a compromise requiring less computational demand at the expense of accuracy [26].

An additional study was carried out using the PPTC model-scale propeller to analyse and compare the difference in results produced by a sliding mesh and moving reference frame domain using unsteady methods for one particular advance coefficient value. Table 3 presents the K_T and K_Q for both simulations, allowing

comparison. Results indicated minimal difference in performance between both methods and therefore, being less computationally expensive, the MRF approach was used for all further analyses.

A similar validation study was carried out between steady and unsteady time models for the same propeller, with the latter being typically used for time-dependent simulations or when physical instabilities exist. These models are assigned solvers that control the number of iterations or time step magnitude. As can be seen in

Table 4 there are minimal differences between the two and therefore the optimisation analysis was carried out using the steady model requiring less computational power.

4.3. Mesh generation and grid dependency test

The surface mesh was generated using triangulated faces. For proper and accurate simulation, the generation of an accurate representation of the blade geometry was of great importance. Blade tips and sharp edges were captured accurately indicating feature lines in the modeller. Fig. 4 depicts the surface mesh for the CAESES propeller at full scale.

During the validation stages, three different types of mesh grid refinements were also investigated, classifying them as coarse, medium and fine. Refining the mesh resulted in insignificant differ-

Table 7
Design Variables.

Parameter	Lower Limit	Upper Limit
Length (m)	0.420	0.840
Height (m)	0.062	0.410
Maximum Thickness (m)	0.004	0.080
Pitch (deg)	-50	50
Angular Fin Position (deg)	0	71

Table 8

Calculation of the discretisation error for KT and KQ values (with monotonic convergence).

	KT	KQ
r_{21}, r_{32}	$\sqrt{2}$	$\sqrt{2}$
ϕ_1	0.3862	0.0969
ϕ_2	0.3843	0.0967
ϕ_3	0.3798	0.0960
p	2.4789	3.6147
ϕ_{ext}^{21}	0.3876	0.0970
e_{ϕ}^{21}	0.4920%	0.2064%
e_{ext}^{21}	0.3582%	0.0825%
GCl_{fine}^{21}	0.4494%	0.1032%

ences in the efficiency values. Although the three models produced similar results, the fine mesh (Table 5), was deemed most reasonable being able to capture local flow quantities accurately. For the full-scale analyses, a mesh of around 10 million hexahedral cells was generated selecting a reasonable cell size growth-rate from the inner to the outer field while also specifying local area refinements (Fig. 7) in critical regions.

The presence of a surface or wall boundary significantly affects the flow behaviour producing different turbulent structures from free turbulent flows. Flows near solid boundaries have a substantial region which is dominated by inertia forces and a thinner region, that closest to the wall dominated by viscous forces. The latter is made up of three layers known as the 'linear sub-layer', the 'buffer zone' and the 'log-law layer' in order of increasing distance from the wall and are differentiated due to the kind of stresses that dominate; The linear sub layer is dominated by viscous stresses, the buffer layer is a balance of viscous and turbulent flow and the log-law layer is dominated by Reynolds (Turbulent) stresses.

Due to the complexities and effects in the boundary layer, the mesh in this region should be refined in order to accurately capture near wall flow details. A prism layer model feature was therefore employed generating refined orthogonal prismatic cells adjacent to the surface with 12 layers. In Star-CCM, the near wall turbulence quantities such as force and velocity are captured using wall treatment models. For this particular study, the All- y^+ treatment approach was used, which is a hybrid that emulates both the Wall Function law approach for y^+ values (y^+ is a non-dimensional wall distance for a wall-bounded flow) greater than thirty and the Near-Wall turbulence for y^+ values lower than one trying to resolve the viscous sub layer. Since the validation study was carried out at model scale, the simulation was modelled in such a way as to mostly avoid y^+ values greater than 1 for enhanced accuracy. This being said, in order to achieve such small y^+ values in full-scale

conditions, a high cell number is required which was not deemed feasible for this study. Therefore, with regards to the full-scale CAE-SES propeller, it was necessary to have the smallest y^+ values but possibly greater than 30 in order to avoid the buffer region. It was therefore deemed appropriate to run model scale simulations with high and also with low y^+ values in order to validate simulations using both the Wall Function and Near-Wall approaches. As can be seen in Table 6, the two methods produced similar results with the lower y^+ simulation giving slightly enhanced accuracy as expected. It was therefore concluded to run the validation at model scale using lower y^+ values (<1) and the full scale study to be carried out using higher y^+ values (>30). Fig. 5 and Fig. 6 below indicate the wall y^+ frequency distribution range for the propeller simulations post completion.

4.4. Boundary conditions

Since boundary conditions influence the nature of a simulation, their appropriate selection is important. A velocity flow was specified for the inlet boundary condition and an atmospheric pressure field for the outlet. The initial flow velocity at the inlet condition was set to the advanced velocity of the water depending on the advance coefficient (J) in question. The cylindrical boundary was set to a symmetry condition simulating open water with no constraints and the submerged propeller was assigned with a no-slip (wall) condition. The positioning of the boundaries is also an important factor that requires consideration, in particular, the upstream inlet boundary and the downstream outlet boundary. These should be defined in a way to avoid any reflections downstream of the propeller and to ensure uniform incoming flow upstream of the propeller. To model boundary independent solutions, the inlet was placed 2 propeller diameter lengths upstream of the propeller and 5 propeller diameter lengths for the outlet. This configuration and arrangement was used for both the validation and optimisation study. Fig. 8 demonstrates the domain configuration and associated boundary conditions.

5. Optimisation

Shape optimization helps give a better insight into the study and enables the design and manufacture of superior products that might offer superior performance and/or save costs.

Optimisation methods can be carried out in various ways: using different algorithms and approaches; defining one or more constraints; seeking a single or multi-objective approach. Processes might also be computationally expensive and time consuming and therefore careful selection for a robust and efficient system is of utmost importance.

There is no general consensus regarding optimal optimisation methods. Each procedure depends on the design task at hand as well as the time and computational power available. Harries [27] outlines the optimisation approach with 2 consecutive phases; exploration and exploitation. The prior indicates the exploration of the design space identifying areas of interest. Once promising candidates have been identified, they are then fine-tuned to produce the best possible result hence exploitation.

Table 9

Sample of Sobol Design Results.

Sobol Designs	Fin Height	Fin Length	Max. Thickness	Pitch	Start Angle	KQ	KT	η_0
Number	(m)	(m)	(m)	(°)	(°)	-	-	-
1	0.32	0.53	0.0610	25.0	53.3	0.0239	0.1244	0.6617
3	0.19	0.58	0.0515	37.5	62.1	0.0239	0.1246	0.6628
17	0.35	0.51	0.0111	34.4	37.7	0.0239	0.1247	0.6637
19	0.22	0.46	0.0396	21.9	46.6	0.0239	0.1244	0.6616
30	0.08	0.64	0.0349	28.1	33.3	0.0239	0.1240	0.6616

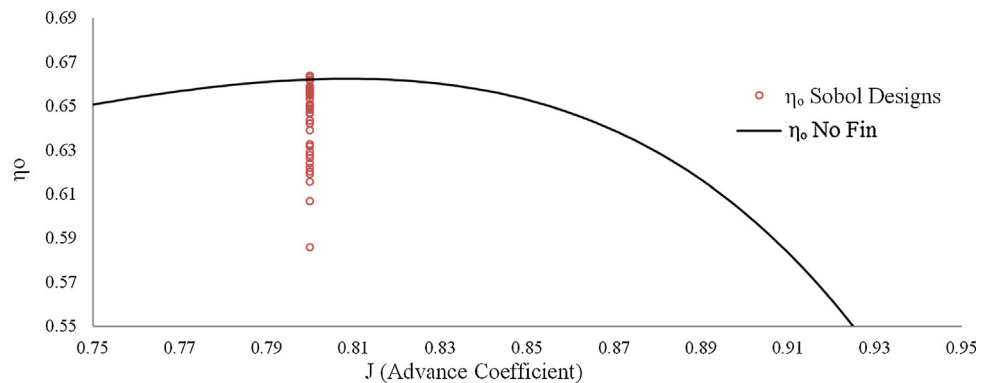


Fig. 14. Quasi Random Designs.

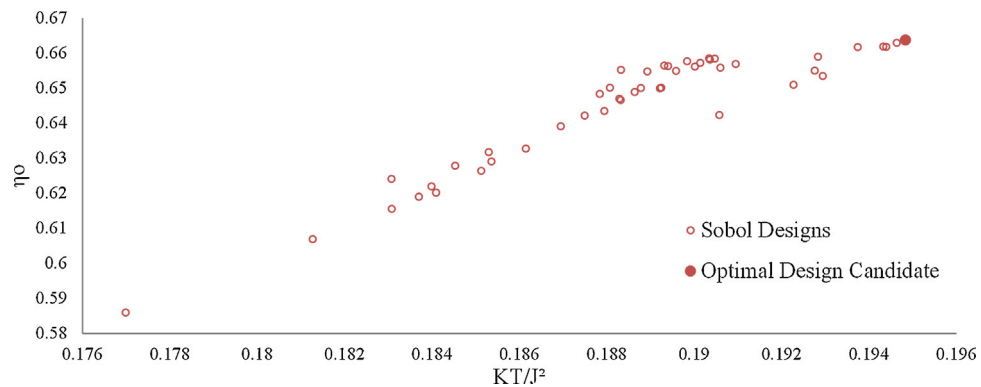


Fig. 15. KT Optimal Design Candidate.

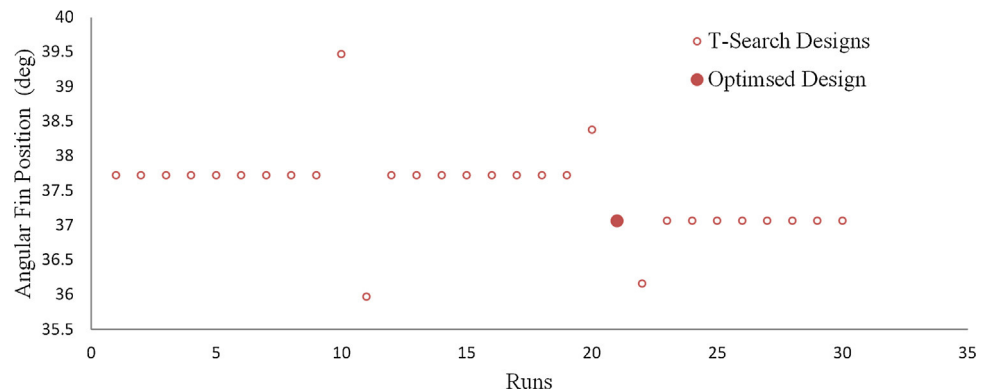


Fig. 16. KQ Optimal Design Candidate.

Exploration helps identify regions of interest in the design space including promising variants also allowing the understanding of design trends while also evaluating any sensitivity involved. For full potential benefits of design exploration in a 3D space environment, x number of design variables would require 3^x number of variants to be investigated that can accumulate to a high number of required simulations. Since this can be very time consuming, other strategies have been developed that exclude unnecessary points in the design space. Such an algorithm is called the Sobol Sequence used for this study.

Post the exploration process, optimization strategies are then used to modify and fine tune the variables with the aim of advancing towards optima. Ideally, the search would yield the finding of a global optimum; however resources generally limit the detail required in the optimisation process to do so. Therefore, there is a possibility of not managing to exploit a global optimum; how-

ever this being said, a local optima, one that represents a better candidate than the baseline design is generally determined. The exploitation method used in this study is the Tangent Search Method.

5.1. Procedure

CAESES is a powerful and flexible 3D parametric modeller that can be integrated with a CFD solver to enable design optimisation with post-processing capabilities. For this particular study, CAESES was integrated with Star-CCM+ ensuring proper interaction and file transfer. CAESES has a choice of different algorithms and optimisers built-into the software but only the Sobol and the T-search methods were used for this particular study. These two engines generally complement each other with the Sobol examining a design space (batch design approach) to identify the best

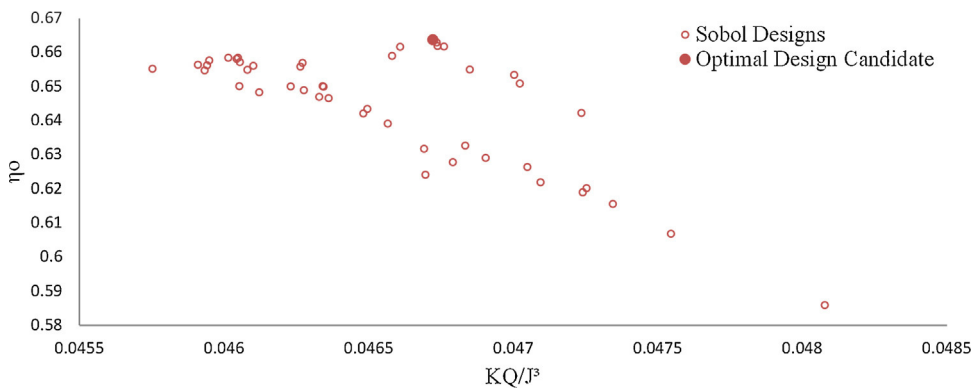


Fig. 17. Angular Fin Position Variations.

Table 10
Energy Efficiency Gain.

Design	KT	KQ	η_0	Increase in η_0 (%)			
No Fin	0.1216	0.0236	0.6563	–			
A	Sobol 0.12470	T-search 0.12468	Sobol 0.02392	T-search 0.6637	Sobol 0.6648	T-search 1.30	
B	0.12457	0.12461	0.02393	0.02392	0.6628	0.6632	1.06
C	0.12437	0.12455	0.02393	0.02394	0.6617	0.6625	0.95

Table 11
Optimal Design Parameters.

Design A				
Height (m)	Length (m)	Thickness (m)	Pitch (deg)	Angular Fin Position (deg)
0.352	0.512	0.0111	34.38	37.06

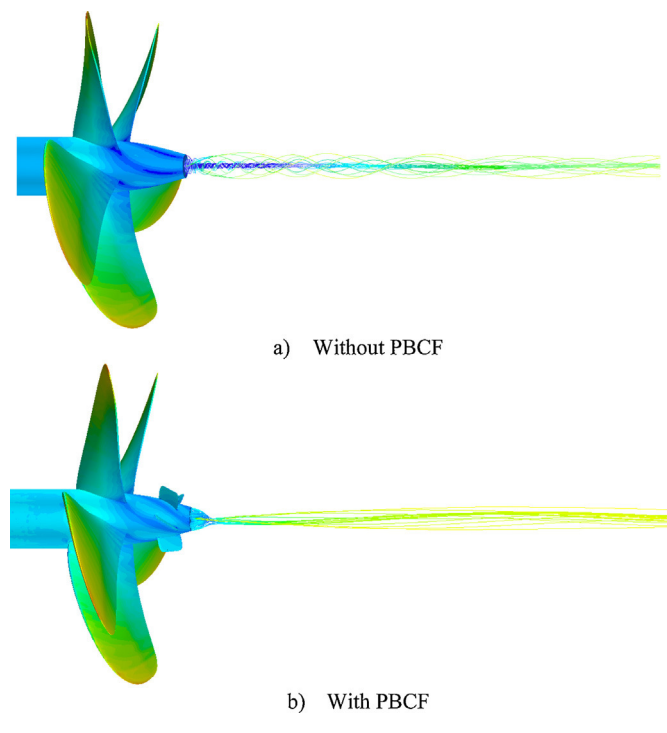
candidates and T-Search analysing those candidates further and modifying them to meet certain goals within specified constraints (optimisation).

The Sobol sequence is a deterministic algorithm of a quasi-random low-discrepancy sequence (Fig. 9) that produces a pattern in the design space that seems random but is somewhat deterministic. It is designed to generate uniform sampling over a design space by generating candidates in regions that are least populated thus avoiding the repetition of the same geometry [28]. On the other hand, random sequences (Fig. 10) tend to produce busy areas as well as voids in the sample space. Quasi-random or low discrepancy sequences are less random than pseudorandom number sequences because they tend to sample space smartly and more uniformly making them more effective for global optimisation. The quasi-random approach generates a more efficient variation than the random sequence over a design space leaving no clusters or voids, hence resulting in better analysis for design exploration [29].

The Tangent Search Method, originally proposed by Hilleary [30], is a gradient free method that features moves similar to those of gradient directions. The T-search method is a reliable optimisation algorithm (Fig. 11) with a single objective goal considering inequality constraints. The algorithm detects a descent search direction in the solution space towards a goal whilst restricting itself to a feasible domain. It applies a direct search method within the pre-defined constraints. The method is based on exploratory moves to find promising search directions in the design space and global moves making steps along the identified directions towards superior designs. Such a method is capable of identifying the local minimum in a solution space [29].

With this study only requiring one objective i.e. improving the propeller efficiency, the following optimisation process was selected. 45 variations using the Sobol engine were first examined. This produced a sufficient spread of designs over the design space.

The three best candidates were analysed further and optimised for 25 iterations, each producing the local optimal designs. These were then compared and the global optimum deduced.



a) Without PBCF

b) With PBCF

Fig. 18. Hub Vortex.

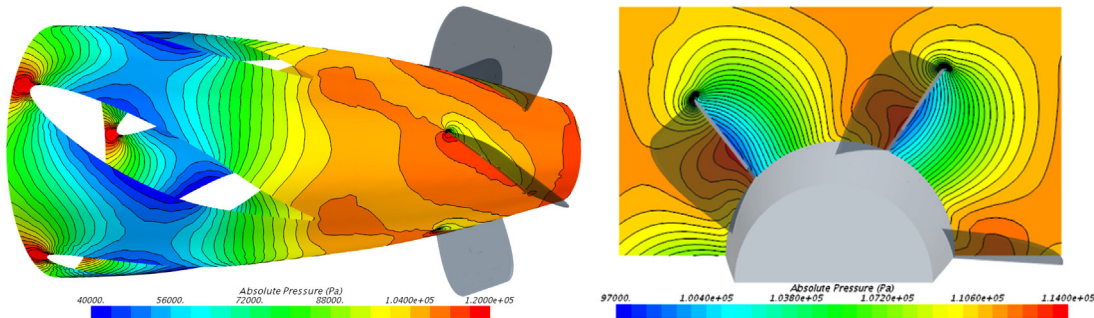


Fig. 19. Pressure Distribution.

Table 12
Performance Breakdown.

	No PBCF	PBCF
Propulsion System	Thrust (N) 1.435×10^6	Torque (Nm) 2.228×10^6
Blades%	100.72	99.99
Hub%	-0.67	0.01
Boss Cap%	-0.05	0.00
PBCF%		0.55

Table 13
Performance Difference after PBCF Installation.

Propulsion Components	Performance Difference	
	Thrust (%)	Torque (%)
Propulsion System	2.50	1.39
Blades	2.47	1.69
Hub	0.01	0.00
Boss Cap	0.58	0.00
PBCF	-0.57	-0.30

5.2. Parametric study

The limiting bounds of the design variables were defined according to the validity of the parametric model as depicted in Table 7.

The Sobol engine was used to generate a total of 45 variations within the limiting conditions of the design space. For each design, the K_T , K_Q and propeller efficiency were computed identifying the better of the designs while also ensuring the validity of the y^+ range.

The best three designs were then assigned to be parent designs requiring further optimisation using the T-search method for 25 iterations each. The reason for not simply carrying out the optimisation analyses using only the best design is due to the room for improvement that can be achieved for each of the three. Prior to optimisation, a parent design might produce less favourable characteristics than another but it might turn out to provide better results after the optimisation process has been carried out reaching the global min/max. After taking into consideration the computational time, power and resources available, a selection of three designs seemed most appropriate.

6. Results

6.1. Validation study

Fig. 12 presents a graph that demonstrates the comparison between experimental and numerical results for the PPTC propeller characteristics. Results yielded satisfactory open water efficiency accuracy of 3% between the advance coefficients (J) from 0.6 to 1; with the accuracy decreasing significantly outside this range. This corresponds well to other authors' outcomes reasoning that this behaviour is a result of the lack of the transition model in the

simulation. The RANS simulation model was set to assume a fully turbulent flow which failed to predict the transition behaviour in the boundary layer.

The accuracy can be improved by either employing a transition model into the simulation or by carrying out open water tests at full scale. The transition region within the boundary layer of a full-scale model is less significant compared to that for a model-scale, thus improving accuracy. Although full-scale simulations minimise errors, as Bhushan et al. [31] indicate, these require a high grid density near the wall which might prove to be computationally expensive and might cause high grid spacing aspect ratios near the wall. This increases errors in the mass, momentum and flux calculations thus requiring the use of wall functions.

6.2. Verification study

A verification study was carried out on the PPTC propeller to demonstrate and ensure the capability of the model and solver using the Grid Convergence Index (CGI). This method is based on Richardson extrapolation [32,33] and is used in this study to calculate the discretisation error estimation as described by [34].

The apparent order of the method, p , is calculated by

$$p = \frac{1}{\ln(r_{21})} |\ln|\varepsilon_{32}/\varepsilon_{21}| + q(p)| \quad (8)$$

$$q(p) = \ln \left(\frac{r_{21}^p - s}{r_{32}^p - s} \right) \quad (9)$$

$$s = 1 \cdot \text{sign}(\varepsilon_{32}/\varepsilon_{21}) \quad (10)$$

where r_{21} and r_{32} are refinement factors, i.e. $\sqrt{2}$ in this study, and $\varepsilon_{32} = \phi_3 - \phi_2$, $\varepsilon_{21} = \phi_2 - \phi_1$, ϕ_k is the key variable, i.e. K_T and K_Q in this case, on the k^{th} grid.

The extrapolated values are obtained by

$$\phi_{ext}^{21} = (r_{21}^p \phi_1 - \phi_2) / (r_{21}^p - 1) \quad (11)$$

The approximate and extrapolated relative errors are calculated using the following equations, respectively.

$$e_a^{21} = |\frac{\phi_1 - \phi_2}{\phi_1}| \quad (12)$$

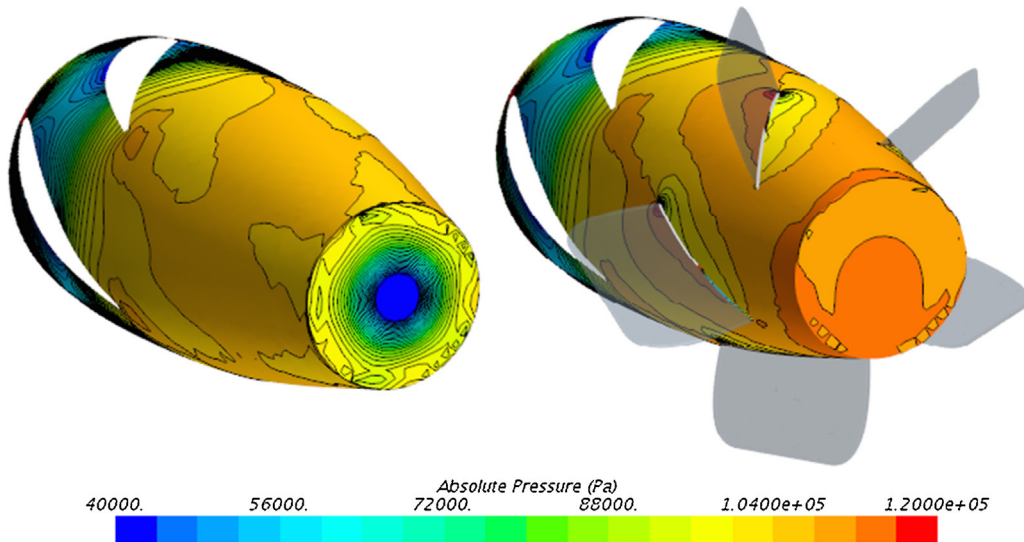


Fig. 20. Boss Cap Tip Pressure Drop.

$$e_{ext}^{21} = \left| \frac{\phi_{ext}^{12} - \phi_1}{\phi_{ext}^{12}} \right| \quad (13)$$

The fine-grid convergence index is calculated by

$$GCI_{fine}^{21} = \frac{1.25e_a^{21}}{r_{21}^p - 1} \quad (14)$$

These parameters were calculated for KT and KQ values and are presented in [Table 8](#).

As can be seen from [Table 8](#) insignificant numerical uncertainties (0.4494% for KT and 0.1032% for KQ) was estimated for the computed values.

6.3. Full-scale propeller analyses

Although, validation was carried out at model-scale with the Potsdam propeller geometry, the CAESES propeller was analysed in full scale conditions in order to produce more accurate results. As seen in [Fig. 13](#), the CAESES propeller was first numerically analysed without any PBCF over a range of J values in order to analyse the propeller performance and identify a propeller operating point for the PBCF optimisation. A suitable condition was found to be at $J=0.8$, which is in between the accurate range of the simulation as previously indicated in the validation study. Various PBCF designs were then installed on the CAESES propeller, simulated at the operation point ($J=0.8$) and compared with the no fins condition.

6.3.1. Quasi-Random designs

[Fig. 14](#) indicates the results of the 45 installed fins generated by the Sobol engine with respect to the no-fin propeller condition at the operating speed. For the ease of visual purposes, the graph only indicates from 0.75 to 0.95 η_0 , representing the peak of the open water efficiency curve in order to be able to identify the better designs. Most of the designs were detrimental to the open water efficiency, with only a few of them resulting in beneficial results. Promising candidates indicated a potential propulsion efficiency benefit of up to 1%. [Table 9](#) presents a few selected cases of the analysed designs showcasing the parameter values and the associated results. It can be seen in [Fig. 15](#) that the best design candidate produces the highest thrust. However, it is noted in [Fig. 16](#) that this design does not feature the lowest torque. Thus this indicates that the 2.5% gain in KT outweighs the expense of 1.4% increase in KQ resulting in a 1% net efficiency gain. These outcomes are not

in agreement with other authors' works [5,35] who state that the enhanced efficiency is a result of an increased KT and a decrease in KQ. This could be due to a number of reasons such as different geometry configuration, scale effects and also behind- propeller conditions. Results from this study have however indicated that the best design candidate in full scale open water conditions produced a significant gain in KT outweighing the increase in KQ. This could be due to the fact that the thrust produced is larger at full-scale Reynolds number [5]. This therefore opens a door to an area which requires further investigation.

Other deductions that have been concluded from the better designs at this point were that the fin pitch angle was of the same orientation and similar value to that of the propeller blades. In addition, the circumferential angular position of each fin was best suited to be like that of the blades. Three optimal candidates were then identified for further analyses using an optimisation algorithm.

6.3.2. Optimisation study

These candidates were named A, B and C in descending order of favourable open water characteristics. They were optimised further for 25 iterations using the T-search method. After the optimisation process, design A resulted to be the best design from the analysis. Results indicated that optimising the candidates only resulted in fine tuning the angular fin position as can be seen in [Fig. 17](#). The optimiser also varied the other parameters independently which did not produce any better results. This can be seen in [Fig. 17](#) where the angular fin position remained constant. [Table 10](#) demonstrates the optimal open water efficiency gained by the three designs post the T-search analysis when compared to the no PBCF condition. Therefore, after analysing 120 PBCF designs, the maximum energy efficiency gained by using such a process resulted to be 1.30%. It should be noted that 1% of the net gain was achieved using the quasi-random batch design analyses (Sobol) and the other 0.3% by using the optimisation algorithm (T-search).

[Table 11](#) represents the design parameters for the optimal PBCF (A).

6.3.3. Hub vortex

Other than just providing favourable open water characteristics, a PBCF can also help reduce the hub vortex. As explained by Atlar et al. [7], this wastes a lot of energy as it introduces an adverse, strong swirl into the propeller slipstream. In addition a hub vortex can also lead to rudder cavitation and cause undesirable vibration

and noise. Fig. 18 demonstrates the beneficial effect of the PBCF (optimised A) by reducing the hub vortex downstream of the hub.

Atlar et al. [7] explains the formation of this vortex by breaking it down to two types of flow i.e. primary and secondary. The former is caused by the inversely magnified values of tangential water velocities around the hub and the latter is generated as a result of the moving flow on each side of the blade creating differences in pressure and thus generating a vortex element at each blade root. The latter can be clearly seen in (Fig. 18a). In addition, it was indicated that the viscous boundary layer caused by the frictional drag also contributed to the secondary flow and hence the vortex. Further to this, Funeno [36] points out that the shape or form of the boss cap also has an effect on the performance characteristics of a propeller and carries out a study to analyse the flow around a boss cap and hub vortex using CFD techniques, by comparing a truncated boss cap with a cone type geometry. The truncated shape produced a smaller maximum vorticity hub vortex with a lower minimum pressure, leading to a weaker vortex and better propeller efficiency.

6.3.4. Pressure distribution

The propulsion system has also been analysed for pressure distribution as can be seen from Fig. 19. The figures show a pressure drop on the suction side (right) of the boss cap fins indicating that they are actually producing a lift force in the opposite direction to that of the propeller thrust hence generating a drag. The propeller efficiency improvement of the system can be therefore assumed to be coming from the interaction effects of the propeller with the PBCF. It was deemed necessary to look into the performance breakdown of the propulsion system in order to understand the changes in the system behaviour with and without the fins.

6.3.5. Propulsion system performance Breakdown

Table 12 presents the performance breakdown of each component in the propulsion system as a percentage outlining their contributions in terms of thrust and torque to the system before and after the fins were installed. A positive value indicates a force/moment in the same direction of the propulsion systems' thrust or torque and a negative percentage subsequently indicates the opposite. For example, if one looks at the thrust ($1.435 \times 10^6 N$) of No PBCF condition, it can be understood that the blades are generating a higher thrust ($100.72\% \times 1.435 \times 10^6 N$) than that net force produced by the propulsion system that is subsequently reduced due to the resulting drag of hub and boss cap. As expected for both the PBCF and No PBCF conditions, the blades produced most of the thrust and torque with the hub generating a negative thrust (drag) and a negligible torque. However, at the No PBCF condition, the boss cap produced minimal drag, which was then converted to thrust once the fins were installed.

Table 13 outlines the change in performance of each propulsive component after PBCF installation as percentages of thrust and torque values of the baseline propulsion system (No PBCF condition). Once the fins were installed, the total propulsion system produced net values of 2.5% additional thrust and 1.39% more torque than the corresponding NO PBCF condition. In order to further understand where these increments came from, the performance of each component was analysed individually and compared to its own performance prior the installation of the fins. The following deductions were identified:

- The significant differences come from the blades themselves generating +2.47% and +1.69% higher thrust and torque respectively.
- The installation of the fins introduced a drag (-0.57%) as depicted in Fig. 19 but are however reducing the torque (-0.30%) of the system.

- The boss cap goes from creating a drag to producing a thrust (+0.58%).

The difference in behaviour of the boss cap was considered interesting. This could only be justified by the disappearing low-pressure gradient at the tip of the boss cap once the fins were installed as shown in Fig. 20. This pressure drop occurs at the same location where the hub vortex is generated and could be the cause for a generated lift in the opposite direction of the thrust. In summary, an additional outcome from this study has therefore indicated that the propeller efficiency improvements do not come from the fins themselves but from the interaction effects resulting in performance differences of the blades and boss cap. This statement however requires further investigation and justification.

7. Discussion and conclusions

This paper has demonstrated the benefits of the developed automated optimisation technique which is able to deliver the best designs and maximise results from a system in an easy, quick and effective manner. The proposed methodology can be applied to different case studies and modified to suit different scenarios. This paper exhibits the capability and process for designing PBCF using numerical methods and optimisation procedures, enabling the identification of optimal designs for different case studies and situations. After analysing 120 different PBCF designs, using a quasi-random batch method together with an optimisation algorithm approach, a particular PBCF design was identified to produce an open water efficiency improvement of 1.3% compared to that of a propeller without PBCF. This however, does not imply that this particular design would be optimal for all case scenarios; each ship form and propeller results in different ship flow patterns, thus requiring tailored optimal models. Although this study focused on the optimisation of PBCF, the same process and methodology can be applied to different energy saving devices or case studies to suit different requirements.

Previous studies have shown that PBCF are capable of producing higher efficiency gains than that indicated in this study, especially with regards to controllable pitch propellers [37]. This could be due to a number of factors. It should be noted that most of the experimental tests and numerical simulations have been carried out at model scale. As previously discussed, the laminar flow plays a significant part in model scale conditions while full scale scenarios generate fully turbulent flow with insignificant laminar regions. Generally the scale effect is accounted for by making use of empirical formulae which can prove to be unreasonable or inaccurate as indicated by Funeno [36]. For more accurate simulations, all the analyses for this study were carried out at full-scale which might explain the differences in the outcomes. That being said, this statement requires further verification. In addition this study did not take into account any cavitation modelling that might influence the propulsion efficiency characteristics of a propeller; this could be another valid reason for the discrepancy.

By considering the factors mentioned above, it might be worthwhile to extend this study by adding more design variables, such as boss cap design parameters together with its shape. Furthermore, as previously mentioned, outcomes from this study indicated that the benefits of PBCF did not come from the fins themselves but from the interaction effects resulting in performance differences. This area requires further investigation and justification. Additionally a multi-objective optimisation approach could be used to seek a geometry providing maximum energy efficiency and a reduction in hub vortex cavitation; which might result in different optimal fin geometry all together. Further to this, recent studies [35] demonstrated that the presence of the rudder behind the pro-

peller significantly affects the results. Therefore future work on the research presented in this paper should include the installation of PBCF on the stern of a ship in self-propulsion conditions that might result in enhanced function. The incoming flow in open water tests is uniform in contrast to the case for hull-stern conditions, which might result in different optimal PBCF designs. The results, variance and function for the designs in different conditions could therefore be compared and understood. Since cavitation adversely affects propeller characteristics, more effort will be focused on implementing a cavitation model into the open water simulation. As evidenced by Tezdogan et al. [38] ship motions could also be effectively modelled using CFD. Therefore, another sophisticated study would be to carry out the optimisation of PBCF on the stern of a ship under wave conditions.

Acknowledgements

The authors are grateful for the EPSRC support for the project on 'Shipping in Changing Climates' (EPSRC Grant No. EP/K039253/1) which enabled them to carry out the research reported in this paper. The underlying data in this paper is openly available from the University of Strathclyde data repository at: <http://dx.doi.org/10.15129/5092c712-b3f9-48b1-b91a-213945a65aa3>

It should be noted that results were obtained using the EPSRC funded ARCHIE-WeSt High Performance Computer (www.archie-west.ac.uk). EPSRC grant no. EP/K000586/1.

The authors gratefully acknowledge the technical support team of CAESES for aiding in setting up the optimisation procedures.

References

- [1] The Marine Environment Protection Committee Resolution. MEPC. 203 (62); 2011.
- [2] M. Stopford, *Maritime Economics*, 2008.
- [3] International Maritime Organisation Second IMO GHG study 2009. London, UK; 2009.
- [4] N. Rehmatulla, Assessing the Implementation of Technical Energy Efficiency Measures in Shipping, UCL Energy Institute, 2015.
- [5] T. Kawamura, K. Ouchi, T. Nojiri, Model and full scale CFD analysis of propeller boss cap fins (PBCF), *J. Mar. Sci. Technol.* (2012) (Japan).
- [6] H.R. Hansen, T. Dinham-Peren, T. Nojiri, Model and full scale evaluation of a 'Propeller Boss Cap Fins' device fitted to an aframax tanker, *Symp. Mar.* (2011).
- [7] M. Atlar, G. Patience, An investigation into effective boss cap designs to eliminate propeller hub vortex cavitation. Proceedings of the 7th International Symposium on Practical Designs of Ship and Mobile Units 1998; 757–769.
- [8] B. Schuiling, The design and numerical demonstration of a new energy saving device, 16th Numerical Towing Tank Symposium (2013).
- [9] K. Mizzi, M. Kim, O. Turan, P. Kaklis, Issues with energy saving devices and the way forward, in: *Shipping and Changing Climates*, Glasgow, 2015.
- [10] V. Bertram, *Practical Ship Hydrodynamics*, 2nd ed., Butterworth-Heinemann, 2011.
- [11] C.Y. Hsin, B. Lin, C.C. Lin, The optimum design of a propeller energy saving device by computational fluid dynamics, *Comput. Fluid Dyn.* (2009).
- [12] P. Queutey, E. Guilmeneau, G.B. Deng, F.A. Salvatore, comparison between full RANSE and coupled RANSE-BEM approaches in ship propulsion performance prediction, in: *Proceedings of the ASME 2013. 32nd International Conference on Ocean, Offshore and Arctic Engineering*, Nantes, France, 2013.
- [13] M. Nakisa, M.J. Abbasi, A.M. Amini, Assessment of marine propeller hydrodynamic performance in open water via CFD, in: *The International Conference on Marine Technology*, Bangladesh, 2010.
- [14] L. Da-Qing, Validation of RANS predictions of open water performance of a highly skewed propeller with experiments, *Conference of Global Chinese Scholars on Hydrodynamics* (2002).
- [15] Y. Arikhan, A. Drogul, F. Celik, Performance analysis and investigation of the slipstream flow of potted propellers, *Brodo Gradnja* (2012).
- [16] V. Krasilnikov, J. Sun, K. Henning Halsee, CFD investigation in scale effect on propellers with different magnitude of skew in turbulent flow, in: *First International Symposium on Marine Propulsors*, Norway, 2009.
- [17] Y.K. Demirel, M. Khorasanchi, O. Turan, A. Incevik, M.P. Schultz, A CFD model for the frictional resistance prediction of antifouling coatings, *Ocean Eng.* 89 (2014) 21–31.
- [18] Y.K. Demirel, M. Khorasanchi, O. Turan, A. Incevik, A parametric study: hull roughness effect on ship frictional resistance, in: *Proceedings of the International Conference on Marine Coatings*, London, UK, 2013.
- [19] Y.K. Demirel, M. Khorasanchi, O. Turan, A. Incevik, CFD approach to resistance prediction as a function of roughness, in: *Proceedings of Transport Research Arena Conference*, Paris La Defense, France, 2014.
- [20] H. Ghassemi, A. Mardan, A. Ardestani, Numerical analysis of hub effect on hydrodynamics performance of propellers with inclusion of PBCF to equalize the induced velocity, *Polish Maritime Res.* (2012).
- [21] MOL Techno-Trade Ltd PBCF Department <http://www.pbcf.jp/>. (Accessed 12 October 2015).
- [22] SVA Potsdam Model Basin. Potsdam propeller test case. Potsdam; 2011.
- [23] CD-Adapco. STAR-CCM+ user guide Version 9.0.2; 2014.
- [24] International Towing Tank Conference (ITTC) Practical guidelines for ship CFD applications; 2011.
- [25] J.H. Ferziger, M. Peric, *Computational Methods for Fluid Dynamics*, Springer, 2002.
- [26] P. Kellet, O. Turan, A. Incevik, A study of numerical ship underwater noise prediction, *Ocean Eng.* 66 (2013) 113–120.
- [27] S. Harries, Practical shape optimisation using CFD, *Friendship Systems*, 2015.
- [28] W.H. Press, S.A. Teukolsky, W.T. Vetterling, B.P. Flannery, *Numerical Recipes: the Art of Scientific Computing*, 3rd ed., Cambridge University Press, New York, 2007.
- [29] Friendship Systems Friendship Framework. User manual.
- [30] R.R. Hilleary, *The Tangent Search Method of Constrained Minimization*, Naval Postgraduate School, Monterey, CA, U.S., 1966 (p. 190).
- [31] S. Bhushan, T. Xing, P. Carrica, F. Stern, Model- and full-scale URANS simulations of athena resistance, powering, seakeeping, and 5415 maneuvering, *J. Ship Res.* 53 (2009) 179–198.
- [32] L.F. Richardson, The approximate arithmetical solution by finite difference of physical problems involving differential equations, with an application to the stresses in a masonry dam, *Trans. R. Soc. Lond.* 210 (1911) 459–490.
- [33] L.F. Richardson, J.A. Gant, The deferred approach to the limit, *Trans. R. Soc. Lond.* 226 (1927) 636–646.
- [34] I.B. Celik, U. Ghia, P.J. Roache, C.J. Freitas, H. Coleman, P.E. Raad, Procedure for estimation and reporting of uncertainty due to discretization in CFD applications, *J. Fluids Eng.- Trans. ASME* 078001-078001-4 130 (7) (2008).
- [35] K. Ouchi, T. Kawasaki, M. Tamashima, K. Hajime, Research and development of PBCF (Propeller Boss Cap Fins) – novel energy saving device to enhance propeller efficiency, *Naval Archit. Ocean Eng.* 163 (1995).
- [36] I. Funeno, *On Viscous Flow Around Marine Propellers, Hub Vortex and Scale Effect*, The Kansai Society of Naval Architects, Japan, 2002.
- [37] H. Wang, *Hub Effects in Propeller Design and Analyses*, Ocean Engineering Department, MIT, 1985 (PhD Dissertation).
- [38] T. Tezdogan, Y.K. Demirel, P. Kellett, M. Khorasanchi, A. Incevik, O. Turan, Full-scale unsteady RANS CFD simulations of ship behaviour and performance in head seas due to slow steaming, *Ocean Eng.* 97 (2015) 186–206.